Short-time induction heat treatment of high speed steel AISI M2: Laboratory proof of concept and application-related component tests

James Damon, Philipp Schüßler *, Fabian Mühl, Stefan Dietrich, Volker Schulze

Institute for Applied Materials – Material Science and Engineering (IAM-WK), KIT Karlsruhe, Germany

HIGHLIGHTS

- Feasibility of short time induction hardening of high strength steels.
- Dilatometric prove of sufficiency of short time hardening cycles.
- Correlation with state of the art transient tempering modelling.
- Transfer of laboratory heat treatmentto industrial induction hardening plant.

GRAPHICAL ABSTRACT
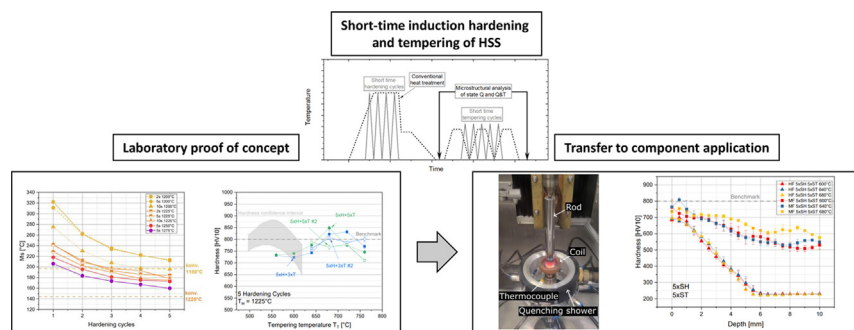
ARTICLE INFO

ABSTRACT

High-speed steels (HSS) such as AISI M2 are generally used for cutting and forming tools or broaches with the highest demands on load bearability and hot-hardness. The requirements for high-speed steels are, on the one hand, extremely high hardnesses of over 800–900 HV and, on the other hand, the thermal stability of the microstructure up to 500 °C. This combination is achieved by complex precipitation-hardenable iron-based alloys. Common heat treatment practices for high-speed steels use salt baths or vacuum ovens, which are energetically unfavorable and require subsequent cleaning. The study consists of short-time hardening and short-time tempering on a laboratory scale by means of dilatometry and thereupon an implementation in an industrial induction hardening machine. The laboratory scale experiments demonstrate the feasibility of bringing sufficient alloying elements into solution by means of several heat treatment cycles despite short holding times of 1 s and less. Combined tests of short time hardening and tempering show a hardness of up to 850 HV10 that are competitive with the conventional heat treatment route. First attempts to transfer the process to an industrial setup exhibit some peculiarities in the process control, but reveal promising results with a surface hardness of up to 750 HV10.

1. Introduction

1.1. Motivation

In order to achieve the best properties in heat treatable steels, high demands are placed on the temperature control of the hard-

ening and tempering process. In the case of high-speed steels (HSS) this applies to the austenitization step at high temperatures above $T_A = 1200\,°C$ for several minutes in order to dissolve the carbide-forming alloying elements in the austenitic phase [1]. The subsequent quenching rate must also be tightly controlled in order to avoid cracking. After cooling, the supersaturated martensite is subjected to a multi-stage tempering heat treatment. Tempering heat treatments at 500–650 °C leads to precipitation of fine (Mo-; W-; V-) carbides with a hardness of 2500–3000 HV,

increasing the overall materials hardness [2] while providing a thermal stability of up to 600 °C [3]. Due to the high demands on temperature control, these components are treated in a vacuum furnaces or salt bath.

By means of induction hardening, heat treatment processes can be carried out efficiently in a matter of seconds. Compared to salt baths, the inductively heat treated parts do require significantly less cleaning. The short-time process of induction hardening offers the potential of processing the entire heat treatment procedure in several seconds to minutes, while the conventional process usually takes up to 6–8 h. While the advantages are evident regarding the rapid and clean heat treatment, the short-term induction heat treatment poses challenges for the adjustment of satisfactory hardness depth profiles. Due to the high heating and quenching rates, high thermal gradients and crack formation can occur [4]. In order to be able to reproducibly adjust favourable hardness values via short-time hardening, a detailed knowledge of the process-structure-property relationship with respect to time and temperature is necessary.

Due to the short process times, homogenization by diffusion is not given sufficient time, resulting in a heterogeneous matrix in terms of element distribution [5] and thus, in the resulting properties after quenching and tempering. While process fluctuations of seconds are negligible in the conventional process, they must be precisely controlled in the case of short-term heat treatment. On the other hand, short-term heat treatments also bring advantages regarding materials engineering, which are characterized, for example, by a graded microstructure (after short-term hardening) with graded properties of a hard surface and a ductile core [6], or also the avoidance of tempering brittleness through short-term tempering [7]. In particular, the avoidance of blue brittleness during tempering leads to an improved combination of hardness and ductility and requires further research attention [8]. The question also arises which time periods and temperatures are necessary to bring a sufficient quantity of alloying elements into solution in order to be able to achieve sufficient hardness in the subsequent tempering process of high-strength steels.

1.2. Conventional heat treatment of HSS

The standard heat treatment for HSS (see Fig. 1) is carried out in a sequence of single or multi-stage preheating steps, holding at austenitization temperatures of 1180 to 1230 °C, quenching and repeated tempering steps at 520 to 600 °C [9]. HSS achieve their exceptionally high hardness from a fine and hard martensite on the one hand and the formation of special carbides containing tungsten and vanadium on the other. Fig. 1 visualises the standard sequence. With increasing austenitization temperature, more carbides (W, V) are dissolved, which contribute to an increase in secondary hardening in the tempering step. The upper limit of the austenitization temperature is specified as 1230 °C. At higher temperatures (≥1250 °C), local melting of carbides accompanied by grain growth may occur [9] (Fig. 2). The tempering treatment is carried out in three cycles with each cycle at the tempering temperature for 1 h before they being quenched to room temperature. The cyclic procedure causes carbon to be bound in precipitates at the tempering temperature, which depletes the retained austenite. Due to the depletion, a fraction of retained austenite transforms into martensite on cooling, which in turn is tempered by the second tempering cycle. The final cooling temperature of each tempering step must fall below the martensite finish temperature, since otherwise metastable retained austenite will remain, which may lead to martensitic transformation and embrittlement [2] during further processing or application. The cyclic tempering heat treatment thus leads to a successive precipitation of carbides, a tempering treatment of the newly formed martensite and a transformation of retained austenite into martensite.

1.3. Short-time heat treatment and carbide precipitation kinetics of HSS

In the pursuit of enabling comparability of varying tempering temperatures and times, equivalent tempering parameters resulting in a correlation of the hardness were developed. A well-known example is the approach by Hollomon and Jaffe [11] with a tempering parameter definition

$$P_{HJ} = T(C + \log(t)), \tag{1}$$

including a material-dependent coefficient C, the tempering temperature T in [°C] and the tempering time t in [h]. According to ASM Handbook of Tool Steels [1], a coefficient of $C = 12.5$ is feasible to compare the tempering hardness of high-speed steels with the tempering parameter P_{HJ}, see Fig. 3. With decreasing tempering time, the tempering temperature leading to a maximum hardness is shifted to higher temperatures. Here, the tempering Parameter P_{HJ} results in a good correlation of tempering temperature and time. A maximum hardness of approx. 850 HV can be achieved by carrying out a tempering process which leads to a tempering parameter of P_{HJ} of 9000–9500. Fig. 3 indicates that the hardness curve after a duration of 0.5 h is not completely coincident with the hardness test series at longer times. Consequently, it can be assumed that a further shift of the maximum hardness peak for shorter heat treatment times to higher P_{HJ}-values may occur, particularly with heat treatment times in the time scale of seconds (See Fig. 4).
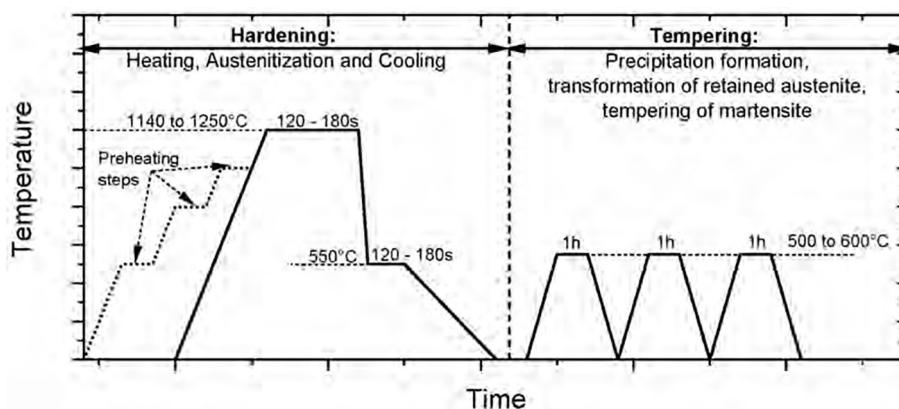

Fig. 1. Schematic time–temperature sequence for hardening and tempering of HSS steels (digitised according to Liedtke [9]).
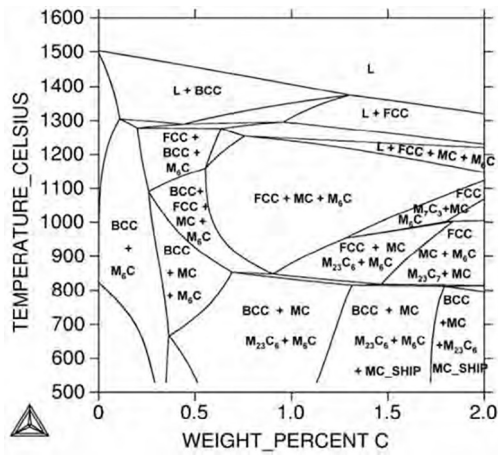
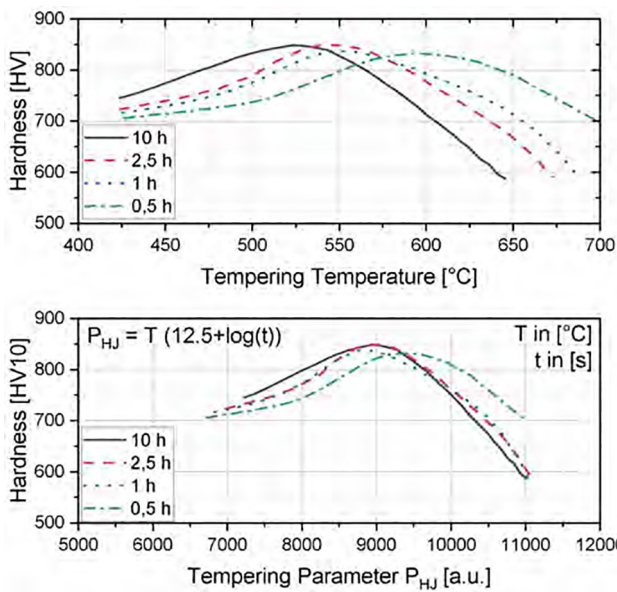**Fig. 2.** Phase diagram of M2 according to Halfa et al. [10].

Fig. 3. Hardness of M2 steel, austenitized at 1220 °C, after tempering. Top: Hardness values after single-tempering in dependence of tempering time t_T, bottom: Calculated tempering parameters P_{HJ} vs. the resulting hardness. Data has been digitized from [1] and recalculated to Vickers hardness HV. The tempering parameter P_{HJ} was calculated with temperature T in [°C] and time t in [s].
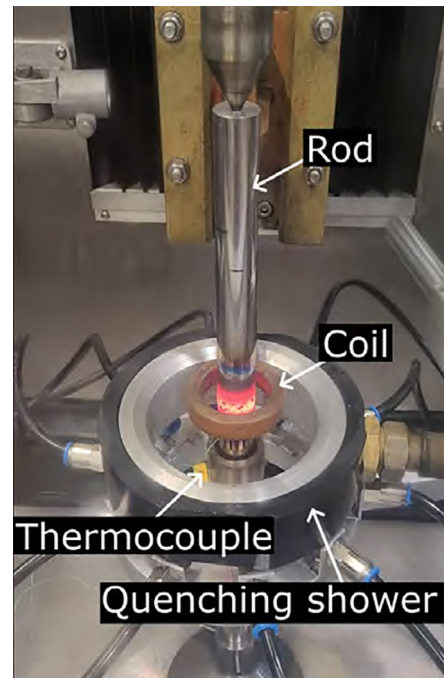

Fig. 4. Representation of the mounting situation of the component (rod) and the induction coil and the quenching shower.

To counteract these discrepancy in the description of Hollomon and Jaffe, various adaptations have been described in the literature [17,20]. All of them have the formulation as an Arrhenius approach in common, where only the proportional effect of time and temperature is evaluated differently. Semiatin et al.[17] describe that a description of the temperature in Rankine ($T^R = 1.8 * T^K$) leads to a better agreement of hardness and tempering parameter.

In order to find out the practical limits of induction hardening of high-speed steels in terms of short-term heat treatment, the effect of continuous temperature control (compared to isothermal steps) at heating and cooling times of a few seconds has to be investigated. To date, no work has systematically investigated the influencing variables of short-time hardening as well as the short-time tempering subsequent to it.

1.4. This work

Within the scope of the work, experiments are carried out on laboratory level by means of dilatometric short-term heat treatment and are characterized in terms of resulting hardness, microstructure morphology and grain size. In addition, the work combines transfer to the shop-floor at an industrial induction hardening facility with component-like geometry. The work aims to understand and optimize the interactions of short-time austenitization and short-time tempering treatment and to create a graded surface layer with a hardness comparable to the conventional process on component level. Finally, incremental Hollomon-Jaffe tempering parameters are determined using the time–temperature curves of the experiments and the resulting material states are compared with the near-equilibrium reference states from the literature.

Studies by Powers and Libsch in the 50s were already able to show the feasibility of short-time induction tempering of conventionally hardened M2 steel [12], but noted that the tempering parameters determined from short-time heat treatment show no correlation with the final hardness. Studies on laser-hardening of M2 steel report a hardness of over 1100 HV and thus illustrate the potential of short-term heat treatments [13]. Recent studies of Sackl. et al. [14,15] reported the feasibility of "short"-time hardening and tempering via dilatometry, using a holding time of 18 s at austenitization temperature. Here, an increase in M_S temperature of 10K was reported, which was consistent with APT measurement where the iron matrix had a reduced carbon content by 0.15wt.% in solution in comparison to the conventional heat treatment state. While recent work on short-time tempering of low-alloy steels often showed good agreement with the Hollomon and Jaffe approach [16–18], the work of Furuhara et al. [19] indicated a significant discrepancy between hardness and tempering parameter for holding times of ≈ 0 s at tempering temperature.

2. Material and methods

2.1. Material

The HS 6-5-2C high-speed steel (often known as M2) is one of the most commonly used high-speed steels. Due to the comparatively low addition of costly elements (W, Mo, V), this steel is cost-effective with excellent toughness and sufficient wear resistance. It will be referred to the chemical composition of the European EN ISO standard as the range of alloying elements is more precise. Table 1 reports the nominal and analysed compositions. The chemical composition is generally within the tolerances, with the exception of slightly reduced Cr contents. For the preliminary tests on a laboratory scale, the wrought material was machined to dilatometric hollow specimens (10 mm length, 4 mm and 3 mm outer/inner diameter). For the induction heat treatment on component scale, rods were machined to a diameter of 21 mm and a length of 200 mm.

2.2. Methods

The DIL 805 dilatometer from TA Instruments was used to examine the short-term heat treatment processes on a laboratory scale (see Section 3). The specimen is heated via induction and the temperature is controlled by a thermocouple type S. The vacuum chamber is evacuated to a pressure of 10^{-4} mbar and flooded with He (99.996% purity) to avoid decarburization or carburization effects.

The induction hardening experiments on component level (see Section 4) were carried out on the FIAND KHM 750 hardening system using an IDEA SMS850 dual-frequency converter [21]. The generator of the hardening system allows a simultaneous dual-frequency inductive heat treatment with a maximum power output of 850 kW with frequency bands of 10–30 kHz for medium frequency (MF) mode and 150–450 kHz for high-frequency (HF) mode. The component surface temperature was recorded using a type K thermocouple in preliminary tests. The repeatability of the temperature curves as a function of the performance data of the induction hardening system was confirmed by multiple tests. The resulting time–temperature curves are shown in Fig. 19.

Microstructural evaluation has been carried out with optical microscopy and scanning electron microscopy after samples were ground and polished to 1 μm and etched with V2A etchant (47.5% hydrochloric acid, 47.5% water and 5% nitric acid) for 30s at 60 °C, to reveal the microstructural features.

Vickers hardness tests (Qness Q20a+) were carried out with a force of 10kg (HV10) in accordance with DIN EN ISO 6507–1 to ensure a reliable analysis.

Phase analysis was carried out by X-ray diffraction (XRD) with a Bruker D2 Phaser using $CuK\alpha$ radiation. The scans were done in a 2Θ range from 40° to 145° with a step size of 0.01° and a count time of 2 s. The dilatometer specimens were ground on the circumference to provide a flat surface for the X-ray analysis. However, the small surface area leads to low intensities. The authors would therefore like to point out that the analyses are used as a comparison among each other and are qualitative in nature.

2.3. Heat treatment procedures: laboratory scale

2.3.1. Short time hardening

In the first step, the influence on the transformation during hardening after short-term austenitization is analyzed. Since constant, isothermal temperature steps can hardly be realized by induction heating on a component scale, the process is carried out by varying the austenitization temperature T_A, heating time t_H to reach T_A and quantity of hardening cycles. The scope of the tests consists of a variation in the austenitization temperature T_A (1100 °C, 1180 °C, 1220 °C, 1250 °C, 1275 °C), the heating time t_H from room temperature to reaching T_A (2s, 5s, 10s) and the amount of hardening cycles (1, 3, 5). The holding time at T_A was set to 1 s, as this ensures a more stable process sequence. This allows to avoid local overheating while ensuring a stable process control for the tests on component scale. The combinations are visualized in Table 2. The transformation kinetics during cooling are investigated, which provides an indication of the alloy elements that have gone into solution in the austenitic phase. In addition, samples states are produced using conventional heat treatment steps for comparison.

2.3.2. Short time tempering

Tests were carried out combining conventional and short time heat treatment in order to investigate the potentials; Conventional hardening (**CH**) with short time tempering (**ST**), as well as short time hardening (**SH**) with conventional tempering (**CT**). Furthermore, promising short time hardening routes were chosen for further investigation in combination with short time tempering. Table 3 lists the procedures.

2.4. Heat treatment procedures: component scale

The thermal history of preliminary dilatometric tests of the most promising states were used as a basis for the component tests using the induction hardening system. Since the induction hardening system can only be controlled by the process time and power, preliminary studies were carried out on the influence of these process parameters on the component surface temperature. The temperature curves of the hardening and tempering tests are addressed in Fig. 19.

3. Results: dilatometry

3.1. Initial material state

Since induction heat treatment processes involve short heating and quenching cycles, the initial or as-delivered condition can have significant effect on the properties after hardening. The as-delivered microstructure of HSS is usually in a soft-annealed condition with a combination of relatively coarse and finely distributed carbides and a resulting hardness of approx. 200-300 HV. In the following Fig. 5(a), the microstructure is shown. The microstructure consists of a ferritic matrix with coarse primary carbides of several micrometers in size. Hardness measurements confirmed a hardness of 220 HV10. The diffraction pattern shows no traces of retained austenite, significant peaks of M_6C-Carbides (Fe3W3C) and peaks of MC-carbides (VC).

Table 1
Nominal chemical composition of M2 tool steel according to DIN EN ISO 4957 and present material composition, determined by means of emission spectroscopy, in wt.%.

Element	Fe	C	Si	W	Mo	Cr	V
HS6–5–2C	Bal.	0.84 − 0.92	⩽0.45	5.9 − 6.7	4.7 − 5.2	3.8 − 4.5	1.7 − 2.1
Measured	Bal.	0.86 ± 0.02	0.33 ± 0.03	6.46 ± 0.08	4.95 ± 0.10	3.6 ± 0.10	1.71 ± 0.03

Table 2
Short time hardening: Investigated process parameter combinations.

Austenitization temperature T_A [°C]	Heating time [s]	1 Cycle	3 Cycles	5 Cycles
1100, 1180	5			√
1200, 1225, 1250, 1275	2, 5, 10	√	√	√

Table 3
Short time hardening and tempering (**SH + ST**): Investigated tempering parameter combinations with the respective tempering temperatures T_T.

Hardening process	Heating time [s]	3 Cycles to T_T [°C]	5 Cycles to T_T [°C]
3 Cycles to $T_A = 1225$°C	$t_H = 5$s	560/600/640/680/720/760	
5 Cycles to $T_A = 1225$°C	$t_H = 5$s		560/600/640/680/720/760

3.2. Hardness of conventionally hardened conditions

In this section, the hardness resulting from the conventional heat treatment process will be determined, which will serve as a benchmark for the analysis of the resulting hardnesses of the short-time heat treatment. The literature survey indicates that the desired hardness after heat treatment for HS6–5-2C is 65HRC ($\approx$ 830 HV). Depending on the requirements in combination of toughness and hardness, a value of 62HRC ($\approx$ 750 HV) can be also be desireable. Samples are subjected to conventional heat treatment at the austenitization temperatures of $T_A = 1180$°C and 1225°C in order to represent the upper and lower limits of common austenitization temperatures. Those samples will be referred to as **CH + CT** (conventional hardening + conventional tempering). The purpose of this is to elaborate the extent to which short-time tempering is competitive to conventional tempering. Preliminary work by Powers and Libsch [12] has already shown promising results, which will be reproduced in the following in our own series of tests. Conventionally hardened and short-time tempered (2 s to T_T, 1 s at T_T, 2 s quenching) conditions are analysed (and will be referred as conv. hardening and short-time tempering (**CH + ST**)). Additionally, the range of hardness from literature ([9]) is visualized in Fig. 6 as grey area. While the CH + CT states (full symbols) lead to the expected hardness with respect to the tempering temperature T_T, the maximum hardness of the short-time tempered CH + ST states (open symbols) is reached at temperatures of 650-700 °C with 850 HV. It can be seen that at high austenitization tem-
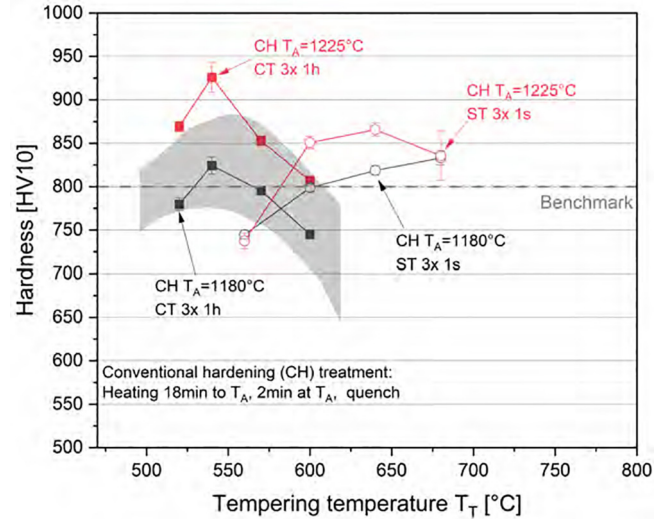

Fig. 6. Hardness vs. Tempering temperature in dependence of the heat treatment process. The maximum of hardness shifts to higher temperatures with less tempering time, while comparable maximum hardness is achieved. Grey area corresponds to the confidence interval of hardness after CH + CT for different batches, according to [9]. For further work, a minimum hardness of 800HV is defined as benchmark, see gray dashed line.

peratures (T_A = 1225 °C), sufficient elements have gone into solution to provide a promising hardness even after heat treatment cycles of a few seconds. Also, under the condition that sufficient alloying elements are brought into solution (by conventional hardening), the short-time tempering can provide promising hardness values. Thus, it can be stated that the major aspect of new investigation should be committed to short-time hardening. In a first step, the mechanisms of short-term hardening on the material state must be understood with respect to conventional hardening.
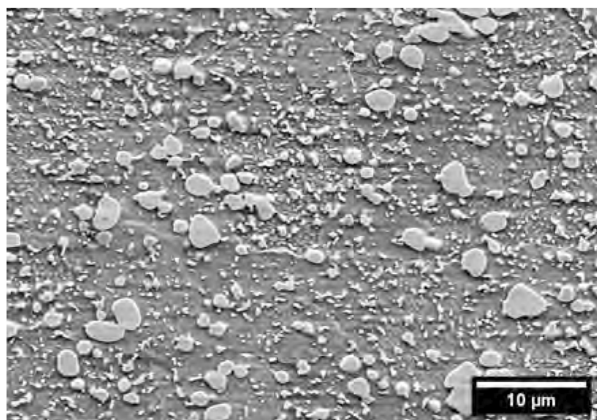
(a) SEM image of the microstructure (etched with V2A).
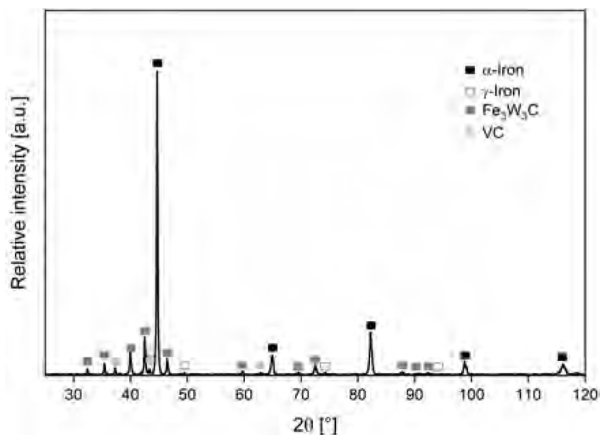
(b) Diffraction pattern.

Fig. 5. Characterization of the delivered and initial, soft annealed material state of M2 high speed steel.

3.3. Analysis of the short-time hardened condition (SH)

3.3.1. Dilatometric analysis

Based on the previous section, the focus is now on clarifying the question as to which means can be used to determine a sufficient amount of elements brought into solution after short-term hardening. In order to reduce the optimization effort, a suitable measure for evaluating the elements that have gone into solution must be determined. Dilatometric screening tests are an excellent method to rapidly analyze heat treatment procedures. As a commonly used evaluation approach, the martensite start temperature can be chosen as a reference, which directly correlates to the alloying elements that have gone into solution. Fig. 7 shows the dilatation curves of the quenching procedure after a CH (conventional hardening) treatment (2 min at T_A = 1180–1225 °C, grey) as well as five cycles of the short-term hardening procedures (red). The local minima of the dilatation curves indicate the beginning of the austenite transformation to martensite. Due to the inhomogeneous nature of the microstructure, high fluctuations of M_S values are given even for the **CH** states. In the case of conventional heat treatment, the martensite transformation starts at approx. $M_S^{1180°C} = 197°C \pm 26°C$ for the lowest austenitization temperature of 1180 °C and reduces to $M_S^{1225°C} = 143°C \pm 24°C$ for $T_A = 1225°C$ and $M_S^{1250°C} = 120°C \pm 16°C$ for $T_A = 1250°C$ when increasing the austenitization temperature, accordingly (see Fig. 7 grey line).

The dilatation curve of the conventional hardening shows a linear shape during cooling, which corresponds to the thermal contraction of the austenitic phase. Deviations from the linear line usually correspond to a phase transformation (to bcc phase) and an associated increase in volume. The conventionally heat-treated specimens report a straight line (hence no martensitic transformation) before reaching M_S. This can be understood as an indicator of how homogeneously the alloying elements are distributed in the microstructure. In contrast, the short-time austenitized curves show an early deviation already at temperatures near 400 °C, indicating an inhomogeneous distribution of alloying elements. For a simplified comparability, the martensite start temperature M_S will be evaluated as the minimum of the dilatation curve. This corresponds to the temperature at which the majority of the microstructure converts to martensite with further under-cooling. As the number of cycles increases, the austenitic transformation kinetics approaches the reference. Despite the short time intervals of a few seconds, successively more alloying elements are brought into solution. In the following, multiple combinations of maximum austenitization temperature T_A, heating time t_H and number of cycles will be evaluated in terms of their martensite start temperature.

Fig. 8 reports the evolution of M_S in dependence of austenitization temperature T_A (1200-1275 °C) and heating time t_H (2-10 s). The holding time of 1 s at T_A is held constant, as the temperature control in the further induction heating process is usually not controlled (and hence, cannot achieve an isothermal holding temperature).

The evolution of M_S temperatures with respect to hardening cycles indicate an exponential decay trend, with high changes of M_S in between the first cycles, approaching a plateau after five cycles. The martensite start temperatures after short-time austenitization at $T_A = 1200°C$ reveal differences between samples in the first hardening cycles depending on their heating time, which remains constant with increasing number of hardening cycles. The short-time tests are close to the martensite start temperature of conventional hardening ($T_A = 1180°C$, yellow horizontal line) after five cycles, with variations between samples of up to 25 K. Here, varying the heating time (t_H = 2 s, 5 s, 10 s, see symbols) shows no significant change in M_S.

In contrast, dilatation curves after heat treatment at 1225 °C indicate excellent reproducibility irrespective of heating time t_H (2 s, 5 s, 10 s). M_S temperatures are reproducible at about 180 °C, but are 35K higher (M_S = 145 °C) compared to conventional heat treatment at $T_A = 1225°C$ (see orange data in Fig. 8).

A second aspect of the study addresses the possibility of provoking overheating by short-term heat treatment and thus, accelerating diffusivity, possibly bringing more alloying elements into solution. The restriction here is to ensure that no melting of carbides occurs. By further increasing the austenitization temperature T_A beyond 1225 °C, even lower M_S values and thus, presumably even higher secondary hardnesses can be achieved after tempering. Heat treating at 1250 and 1275 °C for a heating time of $t_H = 5s$ does lead to slight reductions of M_S values than the material states heat treated at 1225 °C.

3.3.2. Microstructure after short-time hardening

Fig. 9 depicts the resulting microstructure after five cycles heated in $t_H = 2s$ in dependence of the austenitization temperature T_A. Metallographic analysis reveals that the former primary carbides are partially melted with an eutectic structure (see Fig. 9 (d) and 9(e) between the grains). According to the phase diagram
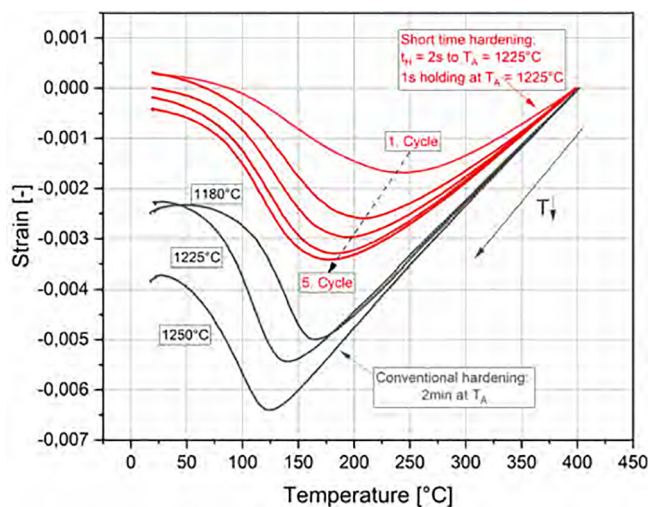
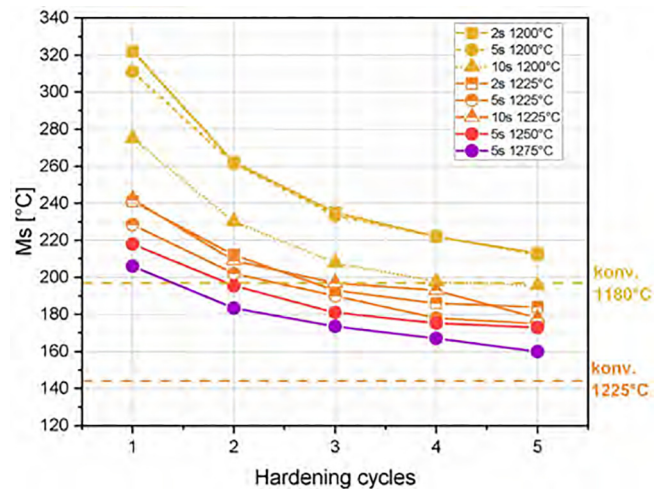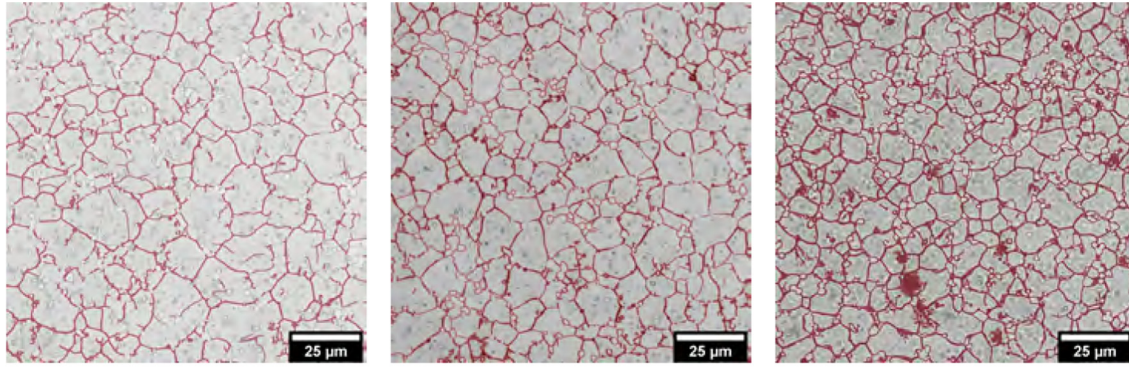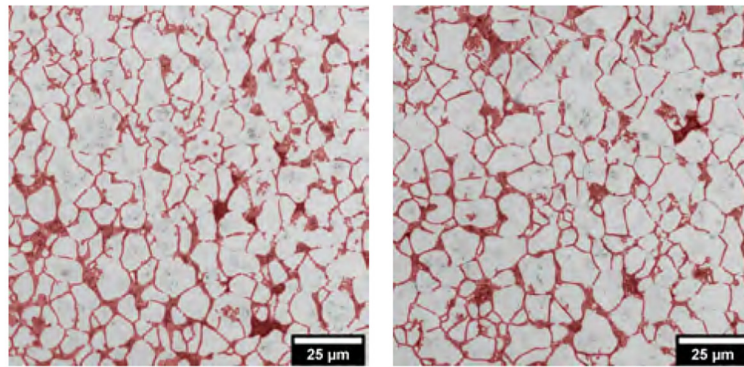**Fig. 7.** Quenching dilatation curves in dependence of the heat treatment.

Fig. 8. Evolution of martensite start temperatures M_S with increasing number of cycles, in dependence of austenitization temperature $T_A = 1200 - 1275 °C$ and heating time t_H = 2–10 s.

(a) Conventional 20min to T_A = 1180 °C, 2min at T_A (b) 5 Cycles, 2s to $T_A = 1200$ °C   (c) 5 Cycles, 2s to $T_A = 1225$ °C

(d) 5 Cycles, 2s to $T_A = 1250$ °C   (e) 5 Cycles, 5s to $T_A = 1275$ °C

Fig. 9. Overlayed micrographs of short-time hardened (SH) samples, in dependence of heating time and austenitization temperature. The grain boundaries and molten ares are highlighted in red.

(Fig. 2), MC and M_6C-Carbides form a liquid phase at temperatures beyond 1245 °C. However, rapid heating procedures with only a few seconds at T_A seem to be sufficient to cause significant melting in the microstructure. With a further increase in temperature, the carbides are successively melted until the phase boundary temperature of 1280 °C is exceeded, where only ferrite, austenite and liquid phase are present. The material state heat treated at 1275 °C (see Fig. 9(e)) shows hardly any remaining primary carbides but eutectical, formerly molten areas between the grains. At austenitization temperatures of 1250 °C and beyond, imperfections in the form of pores/voids can be identified, which are presumably the cause of melting, which will likely have a negative effect on the structural integrity of the components. To limit the scope of the study, the authors chose not to pursue these states further, as on one hand the geometric stability cannot be ensured, and on the other hand the sharp-edged morphology of the remelted carbides could reduce the toughness of the material state.

3.3.3. Prior austenite grain analysis

Fine austenite grains are known to lead to an increase in overall hardness and usually improve the load bearability of components. To investigate the influence of short-term austenitization on grain size, several optical micrographs (see Fig. 9) were analyzed for each condition. The resulting grain sizes are shown in Fig. 10. With increasing austenitization temperature, the grain size increases from about 8–9 μm to 12 μm. The grain sizes are within expected size of conventionally heat treated samples at the same temperature. Thus, it can be stated that short-time hardening (holding time
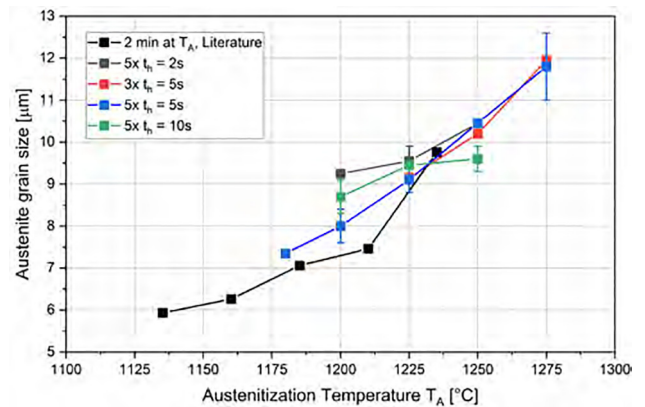

Fig. 10. Final austenite grain size with respect to austenitization temperature, heating times and cycles. Literature data digitized from ASM Handbook Heat treating of iron and steels [1].

of 1 s at T_A) for 3–5 cycles leads to a near-equilibrium state of the austenite grain size. The austenite grain size is limited by the presence of MC and M_6C, which impedes grain growth and thus leads to a fine microstructure. As addressed in the microstructural analysis, melting of the MC/M_6C carbides takes place at temperatures of 1245 °C and higher, leading to a successive coarsening of the austenite grains. However, even at temperatures $T_A = 1275$ °C

(above the solidus line of VC-eutectic) a comparatively fine mean grain size of 12 μm remains.

3.3.4. Conclusion of short-time hardening (SH)

By means of varying the austenitization temperature and the heating time, extensive studies were carried out to determine the M_S-temperature. The study shows that with increasing number of cycles at $T_A = 1225$°C, a plateau of M_S-temperature comparable to a conventional heat treatment of 1180 °C persists, indicating that a similar amount of alloy elements is brought into solution. With austenitization temperatures of 1250–1275 °C, comparable M_S-temperatures to conventional hardening can be achieved, but at the expense of the remelting of the MC/M_6C carbides. Consequently, for the following short-term annealing tests, austenitization is performed at 1225 °C for 3–5 cycles, resulting in a M_S-temperature of 180–200 °C, being comparable to a conventional hardening treatment at $T_A = 1180$°C.

3.4. Analysis of the short-time hardened and short-time tempered condition (SHST)

In the following, the resulting hardnesses after multiple hardening of 3 or 5 cycles at 1225 °C and a subsequent short-time tempering heat treatment are shown (see Fig. 11). The material states after triple hardening lead to a hardness of about 750HV after tempering, regardless of the tempering temperature. Even though one test appears to have reached 800 HV, it can be seen from the repeated tests that there are fundamental fluctuations and that the specified target of 800 HV cannot be achieved reproducibly by triple hardening. In contrast, a hardness of over 800 HV can be reproducibly achieved in the conditions that were hardened five times and tempered three times (5xH + 3xT) (see Fig. 11b).

Compared to conventional hardening, the hardness maxima are shifted to a temperature of 680-720 °C. The benchmark of over 800 HV is also achieved in repeated tests. By further increasing the tempering temperature, the hardness reduces to less than 750 HV, revealing an optimum at temperatures between 650 to 750 °C. Comparing the two plots, the tests with fivefold hardening offer the potential to set competitive hardnesses by inductive short-term heat treatments.

According to the phase diagram (Fig. 2), MC carbides dissolve at 1245 °C, while M_6C are only completely dissolved at temperatures above 1280 °C. Due to the short-term austenitization, the question arises to what extent the dissolution of MC takes place in comparison to M_6C. The evaluation of diffractograms can provide information about the volumetric amount of phases present. In the following diagram (Fig. 12), the diffractograms of the states of a conventional heat treatment are compared with those of short-time heat-treated states. The diffractograms show a similar pattern across the states, with the majority of the peaks explainable by the phases of α-iron and Fe_3W_3C carbide. Some isolated γ-iron peaks can be identified at 49° and 74° and 93° angles, and for the VC at 37° and 69°. In addition, overlapping peaks of the γ-iron and VC exist at 42° close to the α-iron reflex, which are therefore difficult to assign qualitatively. Of particular note are the austenite peaks at 49 and 74°, which appear to occur in isolated states. However, the occurrence of small amounts of residual austenite could not be correlated with an effect on hardness. Accordingly, a statement of the quantitative phase quantities does not seem to be purposeful, which is why reference is made to the results only for reasons of completeness.

In summary, it can be stated that short-term heat treatment only leads to optimum component conditions by precise temperature control. Competitive microstructural hardness compared to conventional heat treatment can be achieved utilizing a short-term heat treatment of five cycles carried out at a austenitization temperature $T_A = 1225$°C and subsequent triple tempering in the temperature interval between 650-750 °C.

4. Results: induction hardening on component level

4.1. Short time hardening

To test the feasibility on an industrial induction hardening system, rods of 20 mm diameter were heat treated using medium frequency (MF) at 10–35 kHz and high frequency (HF) at 100–450 kHz induction hardening procedures. The rods where heated to the maximum temperature in 5s with a constant power setting. Different cooling strategies (water, compressed air + water, compressed air) were investigated to assess crack susceptibility for the induction hardening process routes (Fig. 13). Due to the changes during the heating and the subsequent cooling process (compared to the conventional process route) a holistic approach with multiple cooling rates was used. Route 1 corresponds to a fast
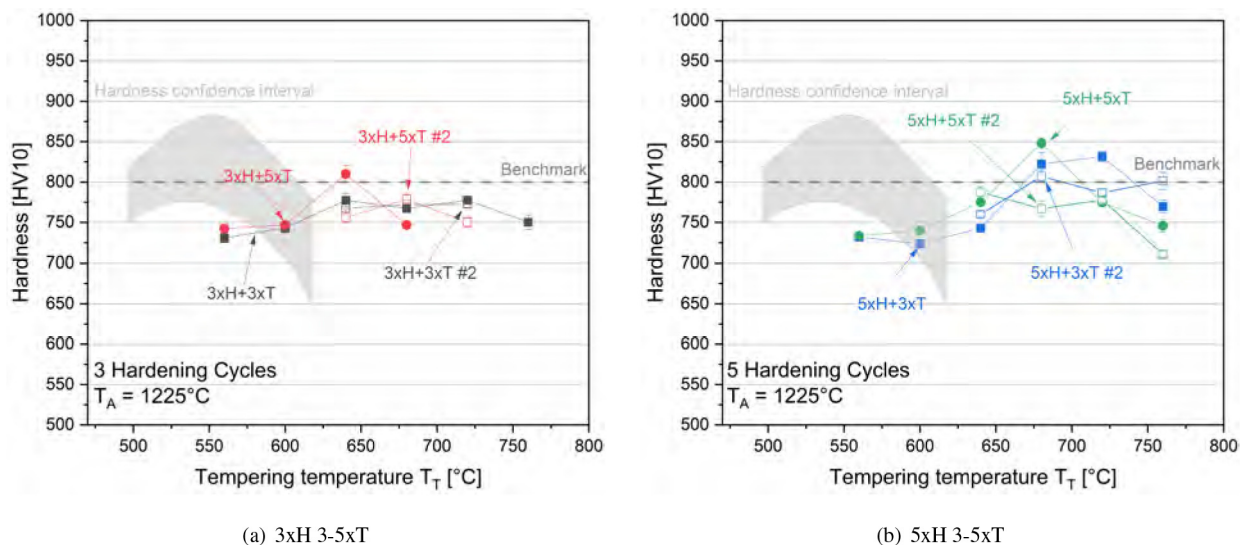

(a) 3xH 3-5xT

(b) 5xH 3-5xT

Fig. 11. Hardness in dependence of tempering temperature of short time hardened and tempered conditions, left: 3 Cycles, right: 5 Cycles. Three Hardening cycles are not sufficient to lead to a hardness after tempering of 800 HV, while five hardening cycles with high tempering temperatures of 680–720 °C lead to hardnesses over 800 HV.
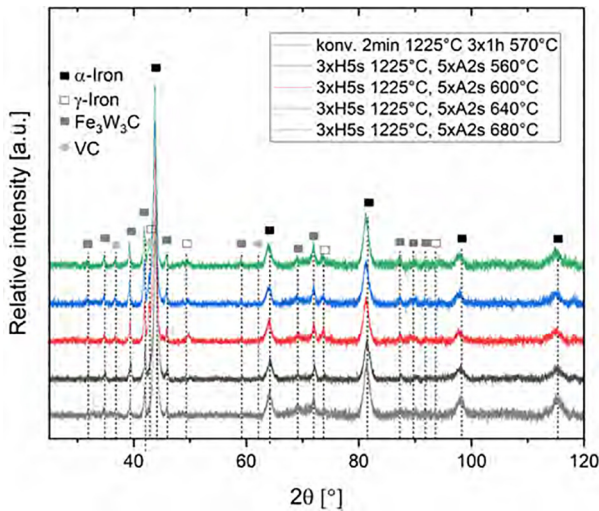
Fig. 12. Heat treatment states analysed by XRD patterns of CH + CT state in comparison to SH + ST state.
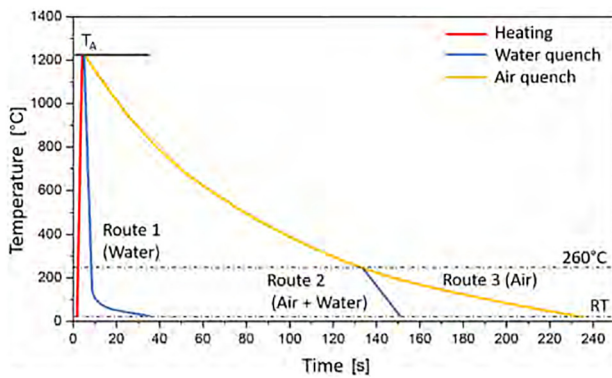

Fig. 13. Experimental temperature profiles.

water quenching with high temperature gradients. In Route 2, compressed air is used for cooling and will be switched to water quenching before reaching M_S at approx. 260 °C. The aim here was to achieve the most homogeneous cooling possible in the component and thus low thermal stress until the martensitic transformation was reached. Route 3 corresponds to the mildest cooling with compressed air until room temperature is reached. Here, the thermal conductivity in the component is high enough to result in a homogeneous temperature across the cross-section during cooling. The comparison of routes 2 and 3 can provide information about the susceptibility to cracking as a function of the martensitic transformation of high speed steels. Conditions following Route 1 (quenched with water) show far-reaching cracks over the entire specimen cross-section in centimeter size (Fig. 14(a)). In a total of four hardening tests (2x MF, 2x HF) all specimens are subject to cracks. The combined air + water quenching (Route 2) also shows cracks in cross-section in all four tested conditions, however, are more isolated and of smaller size (Fig. 14(b)). The sample states of Route 3 (after air quenching) show no signs of cracks (Fig. 14(c)). These are crack-free even after five hardening cycles. The time to cool to room temperature in this case is approx 300 s.

The following image (Fig. 15) depicts the hardness depth profiles up to the center (10 mm) of the threefold and fivefold hardened conditions. In comparison, fivefold hardened rods result in a higher hardening depth after induction hardening with MF (red compared to black) and HF (green compared to blue). The HF con-

ditions show a penetration effect up to 5 mm at which the base material hardness of 230 HV is reached. The MF states show a hardness of about 600 HV in the center, indicating significant penetrating austenitization and solution annealing. At the periphery, the states exhibit hardnesses of 750-825 HV and are thus comparable to the dilatometric hardness results. In the transition region of the HF states, the inhomogeneous microstructure is indicated by the comparatively high standard deviations. It should be noted that the hardness of the hardened-only states offers little information, as hardened states with high proportions of alloying elements contain high proportions of retained austenite and thus, will develop their superior hardness only after tempering.

In addition, the hardness depth curves of the water-quenched variant (W) and the compressed air-quenched variants are shown, even though the water-quenched conditions show strong cracking and are therefore not suitable for further investigation. The hardness depth profiles of air- and water-quenched are near-identical, indicating that the hardness is independent of the selected cooling strategy. Since only the air-quenched samples are crack-free, this cooling strategy will be used for the following tests.

### 4.2. Short time hardening and tempering of rods

In the following, the feasibility of an combined short-time hardening and tempering procedure on an industrial two-frequency system is examined. The states are short-time hardened five times at $T_A = 1225$ °C, each with MF or HF. The number of tempering cycles (3xST/ 5xST) and tempering temperatures T_T are examined as further influencial factors. The resulting surface layer hardnesses are shown in Fig. 16. The depth profiles are similar to the profiles of the hardened states reported in the previous section. Conditions after high-frequency (HF) heat treatment show a graded surface layer condition until they settle into the base hardness of 230 HV at approx. 6 mm. In comparison, the medium-frequency excited states show through hardening with core hardnesses of up to 650 HV. The hardness achieved on the surface are between 675-750 HV for all states and are therefore slightly below the target value of 800 HV.

By variation of the excitation frequency, graded boundary layer states can be produced in the component, which are not feasible by means of conventional heat treatment. This could open up the possibility of defining an optimum which enables optimum wear resistance with high ductility at the same time. In Fig. 17 the microstructure of the HF 5xSH + 3xST 640 °C state is shown. The surface-near region reveals dissolved carbides or remnants of former carbides in form of eutectically solidified areas, which indicate a significant overheating of the surface. In the transition zone (2–6 mm), the primary carbides were partly dissolved, with re-molten primary carbides at the grain boundaries with eutectic appearance. Correspondingly, the grain sizes are also significantly increased. In the transition area of the hardness (between 2–6 mm) a combination of molten primary carbides as well as round, remaining primary carbides can be seen. It can be concluded that the adjusted temperature control led to an unplanned overheating and finally to a coarsening of the microstructure and to a deterioration of the properties.

5. Discussion

5.1. Relationship of temperature and time: The Hollomon Jaffe approach

To better understand the mechanisms of precipitate formation during tempering, the short-term heat treatment results of this
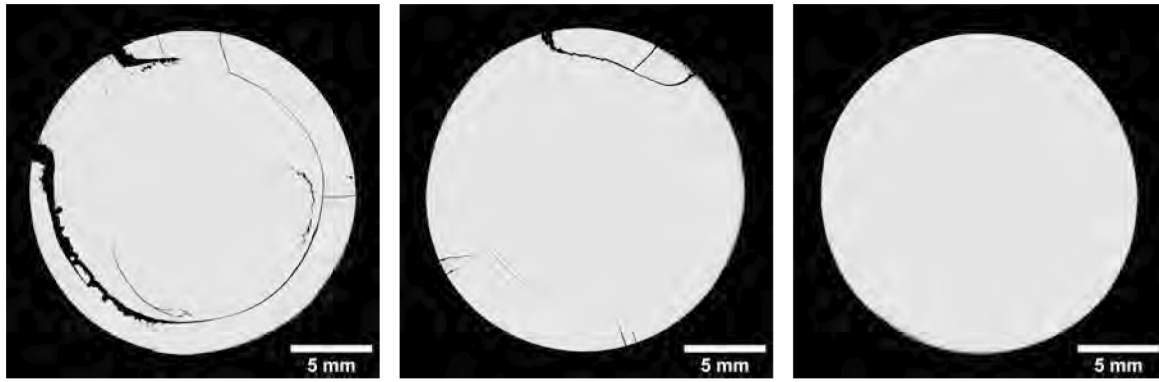
(a) Route 1 (Water)   (b) Route 2 (Air+Water)   (c) Route 3 (Air)

Fig. 14. Segmented metallographic cross sections after different cooling routes: Quenching routes with water quenching will ultimately lead to cracks in the bars. Air cooling led to crack free samples.
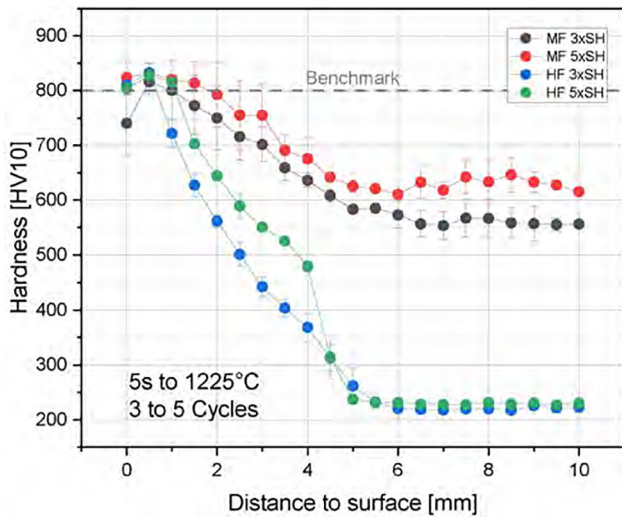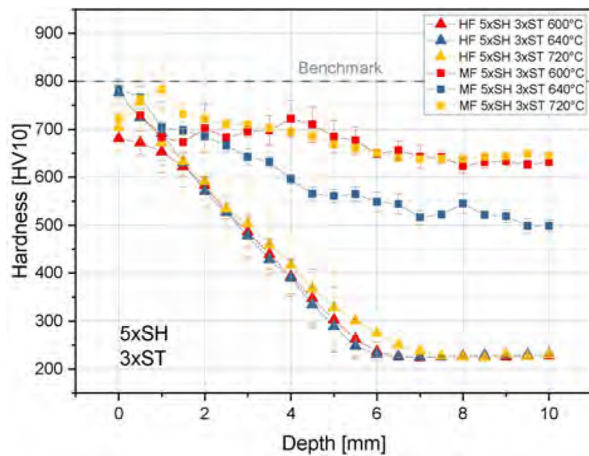

Fig. 15. Hardness depth profile of the induction hardened cylindrical specimens (10 mm = center), induction heated with medium frequency (45–100 kHz) and high frequency (100–450 kHz), quenched with compressed air.

work are compared with literature values. To determine the effective tempering parameter, the non-isothermal temperature curves were approximated using a numerical staircase function. The first step is to analyze the results on a laboratory scale, which are subject to very precise temperature control due to the heat treatment by means of dilatometry. In Fig. 18, the digitized results from the ASM Handbook [1] are compared to the short-time heat treated sample states of this work. The data points of CH + CT are validated by the overall course of the hardness curve in literature (CH + CT (ASM)), that reveals an optimum at a $P_{HJ} = 9000$ with a hardness of 850 HV and more.

In contrast, the states after conventional hardening and short-time tempering treatment show their optimum at values of 8000. Since the short-time annealed curves were heat treated at temperatures up to 680 °C, the effect of temperature on hardness seems to be underestimated by the P_{HJ}. The SH + ST states are difficult to assess due to their uncertain reproducibility in terms of temperature control as well as chemical inhomogeneity, nevertheless, seem to follow a generalized description by the Hollomon-Jaffe-Parameter P_{HJ}.

Within the scope of short time tempering of steels, further approaches of calculating the tempering parameter from the literature (see [17]) were analysed, however, did not lead to an increase
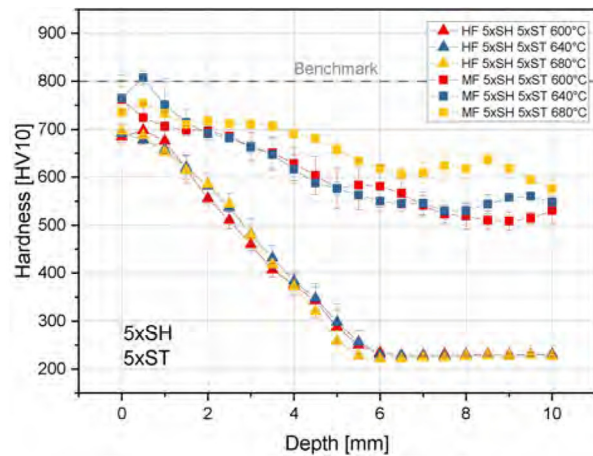
(a) 5xSH 3xST   (b) 5xSH 5xST

Fig. 16. Hardness depth profiles of induction hardened and tempered bars, in dependence of frequency (MF/HF) and maximum tempering temperature. The hardening cycles were carried out at a maximum temperature of $T_A = 1225$ °C. Left: Fivefold hardening and threefold tempering (5xSH + 3xST), right: (5xSH + 5xST).

(a) Surface (Depth ≈ 1 mm)

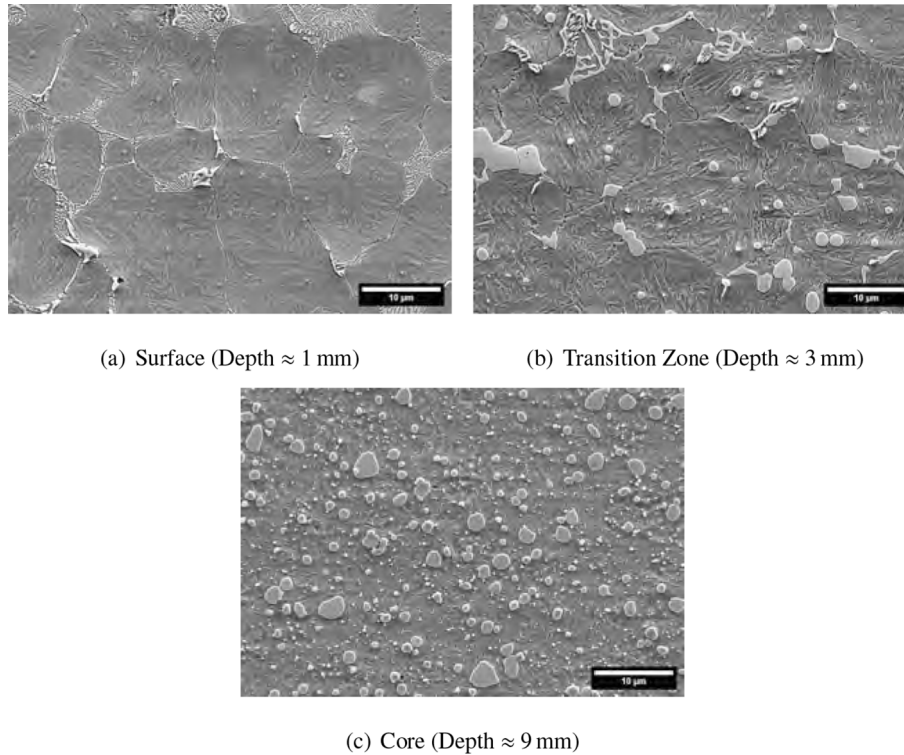(b) Transition Zone (Depth ≈ 3 mm)

(c) Core (Depth ≈ 9 mm)

Fig. 17. SEM images of sample HF 5xSH + 3xST tempered at maximum temperature of 640 °C.
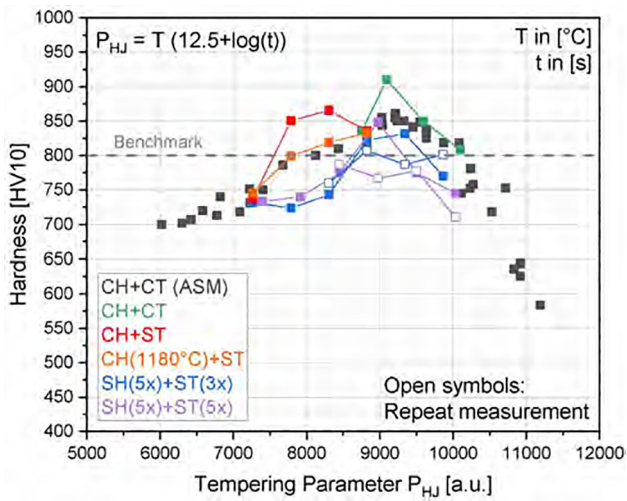

Fig. 18. Calculated Tempering Parameters P_{HJ} vs. the resulting hardness for multiple heat treatment procedures. CH: Conventional hardening, SH: short-time hardening, CT: conventional tempering, ST: short-time tempering.

prediction quality (and hence are not presented here). Furthermore, it should be mentioned that an inhomogeneous microstructure state exists due to the short-term hardening. Here, Sackl et al. [15] reported by means of APT that already by an austenitizing time of 18 s the proportion of dissolved carbon in austenite is reduced by 0.15 wt.% compared to the conventional heat treatment. Therefore, further in-depth studies of the feasibility of short-time hardening for high speed steels must be carried out.

5.2. Resulting hardness on component scale

Due to the transient temperature control in induction hardening operations, precise temperature control (compared to dilatometry) is difficult to realize. Consequently, the temperature control could have a significant influence on the resulting hardness. In Fig. 19, the temperature curves of the bars close to the component in the induction hardening system are compared with the temperature curves of the dilatometric tests. As the induction hardening machine for these experiments was operated by a constant power over time, a perfect temperature control up to 1225 °C can hardly be achieved. Overall, the MF tests reveal a slower cooling rate in comparison to the HF tests, since the component has experienced through heating (as can be seen by the hardness measurements, see Fig. 15). In contrast, the holding time in dilatometric tests of 1 s at T_A is assumed to have a significant impact on the enabled diffusion. After 5 s, the power of the system is switched off and an immediate self-cooling of the component occurs. Hence it can be assumed that during induction hardening, the relevant temperature range of over 1200 °C is only reached for a very short time in order to achieve a suitable uptake of carbide-building elements. Due to the highly complex processes involved in the dissolution of carbides, efforts should be made to develop a time- and temperature-dependent parameter similar to a Hollomon-Jaffe P_{HJ} approach being able to provide a correlation of temperature, time and the quantity of dissolved elements. In addition, future work using dilatometry should analyze a heat treatment that corresponds to the possibilities of induction hardening systems, so that transferability can be made more easily.

6. Summary

In this work, the feasibility of short-time hardening followed by short-time tempering of M2 high-speed steel was investigated on the one hand at laboratory scale (dilatometric) and on the other
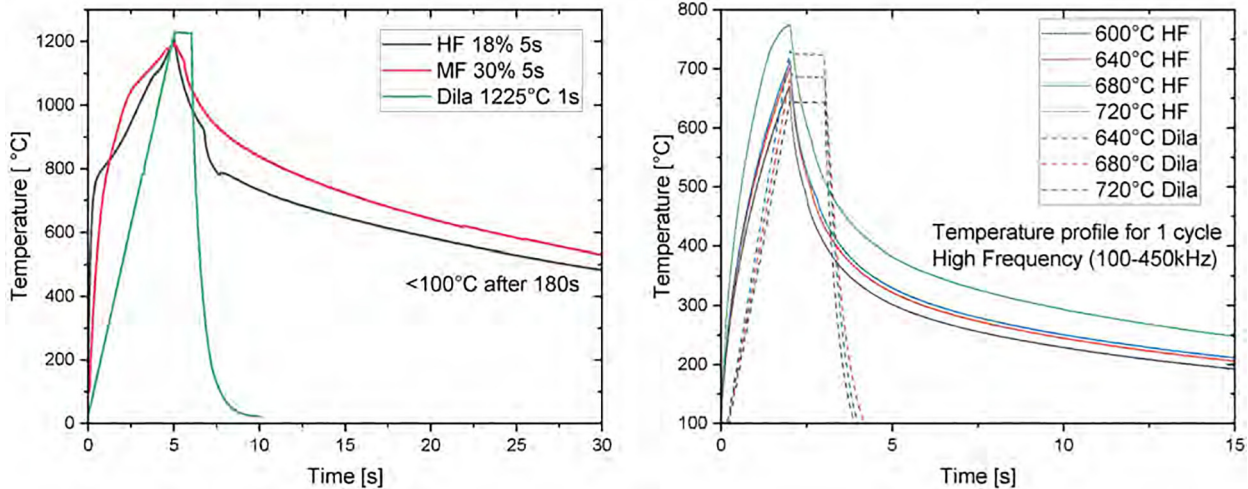
Fig. 19. Temperature profiles of industrial induction hardening plant vs. dilatometrical temperature control. Left: Hardening cycles, right: tempering cycles.

hand at component scale (industrial setup). Through dilatometry, optical microscopy as well as phase and hardness measurements a possible short-time heat treatment strategy for an optimal heat treatment of high speed steels could be developed at laboratory scale. By means of an induction hardening system, repetitive heating and cooling routes were investigated which lead to crack-free specimens and to high hardness, showing the feasibility of induction hardening and tempering even at component scale. This work further reveals:

- Short-time hardening of few seconds is feasible as a solution heat treatment of highly alloyed high-speed steels. With increasing amount of hardening cycles, sufficient alloy elements are brought into solution in order to achieve competitive values of hardness (65 HRC), even with holding times of 1 s and less.
- On laboratory scale (dilatometry), it could be proven that five hardening cycles to 1225 °C and holding for 1 s is sufficient to result in a reproducible hardness of over 800 HV after tempering. Short-time heating to temperatures to 1250–1275 °C for several seconds resulted in molten carbides and grain coarsening, limiting the applicable maximum austenitization temperature to 1225 °C to achieve this level of hardness.
- The tempering parameter according to Holomon and Jaffe can provide a correlation of time and temperature even for rapid tests of several seconds. However, some peculiarities arise with decreased tempering times. The shorter the isothermal treatment becomes, the more the Hollomon-Jaffe approach deviates from isothermal tests.
- Due to the rapid hardening, it can be assumed that an inhomogeneously enriched austenite leads to an inhomogeneous hardness distribution after quenching and tempering. A detailed investigation of the dissolution of elements in HSS with respect to time and temperature seems to be necessary to achieve significant progress in this field.

The transfer of the results to the component level could be demonstrated in the form of crack-free heat-treated rods (similar to broaches), resulting in a surface layer hardness close to 800 HV. SEM results revealed an overheating of the near-surface microstructure of the hardened rods, thus, a highly precise temperature feedback-control on component scale will be necessary to apply the insights from the time–temperature-relationship of microstructures to the industrial application. Nonetheless, by selecting the excitation frequency and heating/cooling rates, it will

be possible in the future to control graded surface layer states for high-speed steels, which on the one hand can exhibit extremely high wear resistance and at the same time retain ductility in the component core.

Declaration of Competing Interest

The authors declare that they have no known competing financial interests or personal relationships that could have appeared to influence the work reported in this paper.

Acknowledgements

References

[1] J.L. Dossett and G.E. Totten, eds., Heat treating of irons and steels, vol. volume 4D of ASM handbook/ prepared under the direction of the ASM International Handbook Committee. Materials Park, OH: ASM International, 2014.

[2] A. Kulmburg, Beitrag zur wärmebehandlung von schnellarbeitsstählen in vakuumöfen, HTM J. Heat Treatment Mater. 46 (3) (1991) 131–136.

[3] J. Schlegel, Schnellarbeitsstahl: ein stahlportraet, Springer Vieweg Wiesbaden, 2022.

[4] P.W. Shelton, A.S. Wronski, Cracking in m2 high speed steel, Metal Sci. 17 (11) (1983) 533–540.

[5] T. Mioković, V. Schulze, O. Vöhringer, D. Löhe, Prediction of phase transformations during laser surface hardening of aisi 4140 including the effects of inhomogeneous austenite formation, Mater. Sci. Eng.: A 435 (2006) 547–555.

[6] D. Kaiser, J. Damon, F. Mühl, B. de Graaff, D. Kiefer, S. Dietrich, V. Schulze, Experimental investigation and finite-element modeling of the short-time induction quench-and-temper process of aisi 4140, J. Mater. Process. Technol. 279 (2020) 116485.

[7] V. Euser, A. Clarke, J. Speer, Rapid tempering: Opportunities and challenges, J. Mater. Eng. Perform. 29 (2020) 4155–4161.

[8] V. Judge, J. Speer, K. Clarke, K. Findley, A. Clarke, Rapid thermal processing to enhance steel toughness, Sci. Rep. 8 (1) (2018) 445.

[9] D. Liedtke, Über das härten und anlassen von schnellarbeitsstahl in theorie und praxis, HTM J. Heat Treatment Mater. 32 (2) (1977) 49–60.

[10] H. Halfa, Thermodynamic calculation for silicon modified aisi m2 high speed tool steel, J. Miner. Mater. Characteriz. Eng. 01 (05) (2013) 257–270.

[11] J.H. Hollomon, Time-temperature relations in tempering steel, Trans. AIME 162 (1945) 223–249.

[12] A.E. Powers, J.F. Libsch, Rapid tempering of high speed steel, JOM 3 (10) (1951) 865–871.

[13] G. Shi, P. Ding, J. Liu, H. Yin, J. Wang, Microstructure and properties of laser surface hardened m2 high speed steel, Acta Metall. Mater. 43 (1) (1995) 217–223.

[14] S. Sackl, G. Kellezi, H. Leitner, H. Clemens, S. Primig, Martensitic transformation of a high-speed tool steel during continuous heat treatment, Mater. Today: Proc. 2 (2015) S635–S638.

[15] S. Sackl, H. Leitner, H. Clemens, S. Primig, On the evolution of secondary hardening carbides during continuous versus isothermal heat treatment of high speed steel hs 6-5-2, Mater. Charact. 120 (2016) 323–330.

[16] S. Murphy, J. Woodhead, An investigation of the validity of certain tempering parameters, Metall. Mater. Trans. B 3 (1972) 727–735.

[17] S. Semiatin, D. Stutz, T. Byrer, Induction tempering of steel: Part i. development of an effective tempering parameter, J. Heat Treating 4 (1) (1985) 39–46.

[18] R. Grange, C. Hribal, L. Porter, Hardness of tempered martensite in carbon and low-alloy steels, Metall. Trans. A 8 (1977) 1775–1785.

[19] T. Furuhara, K. Kobayashi, T. Maki, Control of cementite precipitation in lath martensite by rapid heating and tempering, ISIJ Int. 44 (11) (2004) 1937–1944.

[20] S. Kang, S.-J. Lee, Prediction of tempered martensite hardness incorporating the composition-dependent tempering parameter in low alloy steels, Mater. Trans. 55 (7) (2014) 1069–1072.

[21] F. Mühl, J. Jarms, D. Kaiser, S. Dietrich, V. Schulze, Tailored bainitic-martensitic microstructures by means of inductive surface hardening for aisi4140, Mater. Des. 195 (2020) 108964.